The optimization and scale-up of the electrochemical reduction of CO_2 to formate

Philips, M.F.

Chapter 5

Custom Multipurpose Electrochemical Cell Design and Scale-Up

Introduction

Carbon Dioxide capture and utilization have been gaining attention as a way to combat climate change. There are several ways to convert carbon dioxide into higher-value chemicals. Electrochemical conversion has an advantage over traditional catalysis because it can occur at room temperature and ambient pressure. Additionally, formate has been identified in several studies as an attractive product to pursue from CO_2 electrochemically.[1–5] However, currently, there are no commercial processes for this reaction.

There are several electrochemical configurations that can be used to produce formate from CO_2 (see Chapters 1 and 2 for a discussion and comparison). The current density, current efficiency, and cell potential are key metrics to compare when assessing the technologies. The current density directly affects the capital cost of the process, while the cell potential directly affects the energy costs, and the current efficiency affects both capital and energy costs. Conventional 3D electrodes, trickle flow configurations, and gas diffusion electrodes are the three main configurations researched for this reaction.[6]

3D electrodes have been thoroughly researched and have shown current efficiencies for formate up to 100% at current densities of 56 mA/cm^2.[7] These electrodes convert CO_2 dissolved in an electrolyte, which causes a limitation in their maximum operable current density. This is seen by the current efficiency dropping to 63% at current densities of 95 mA/cm^2 for these electrodes. Trickle flow cell configurations use 3D electrodes but feed a gas-liquid mixture to the cathode. This CO_2 gas/electrolyte mixed feed slightly enhances the mass transfer of CO_2, resulting in current densities up to 294 mA/cm^2 and current efficiencies of 60% for this configuration.[8] However, neither of these technologies can currently achieve as high efficiencies and current densities as gas diffusion electrodes (GDEs). GDEs are porous electrodes that create a three-phase boundary between the electrolyte, CO_2, and the catalyst. This three-phase boundary significantly enhances the mass transfer of CO_2 to the catalyst reaction sites on the electrode and allows for current efficiencies of 75% at current densities ranging from 390 to 500 mA/cm^2 to be achieved.[9,10] For example, the work presented in Chapter 4 discovered a gas diffusion electrode that achieved 99.4% current efficiency at 400 mA/cm^2 for two hours. These are state-of-the-art results when compared to the literature reviewed in Chapter 1 (Figure 1.3).

GDEs are the most promising technology to pursue from a capital cost perspective.[6,11] However, there is not much data published on cell potentials to thoroughly compare the technologies in terms of energy costs. Additionally, the cell potential is dependent on the electrolytes, the cell (current distribution and gap between electrodes), membrane, and anodic reaction, which further convolutes reported data. Furthermore, GDEs are more challenging to scale up as hydrostatic head can become a challenge to maintaining a three-phase boundary. Most reported research on GDEs for this reaction is at a scale of 10 cm^2 or less. This could be a consequence of a lack of commercially available GDE cells. However, larger-scale research is necessary to understand scaling challenges and eventually achieve a commercial process.[12] In this study, a multifunctional 200 cm^2 maximum area cell is designed for GDEs, conventional

3D electrodes, and trickle flow configurations for both the cathode and anode. Furthermore, we use this cell to scale up the best performing electrode formulation found in the set of DOE experiments in Chapter 4.

Experimental

Cell Design

A 200 cm^2 cell was designed in Solidworks for 3D or gas diffusion electrodes at the cathode and anode. The electrochemical cell design is significantly different for a GDE because an extra compartment is required for the gas feed to the GDE. This resulted in our designed cell having up to four compartments. The cell was constructed such that inserts could be used to adjust the active area to any desired size less than 200 cm^2, and flow distributions for each compartment are easily changeable and customizable. Comsol was used to screen flow distributor designs for uniform flow distribution inside the cell. Additionally, multiple cells could be pressed together into one assembly so that experimenting with cell stacks would be possible. A fully assembled cell view is shown in Figure 5.1 with its parts labeled and their material of construction listed in Table 5.1.

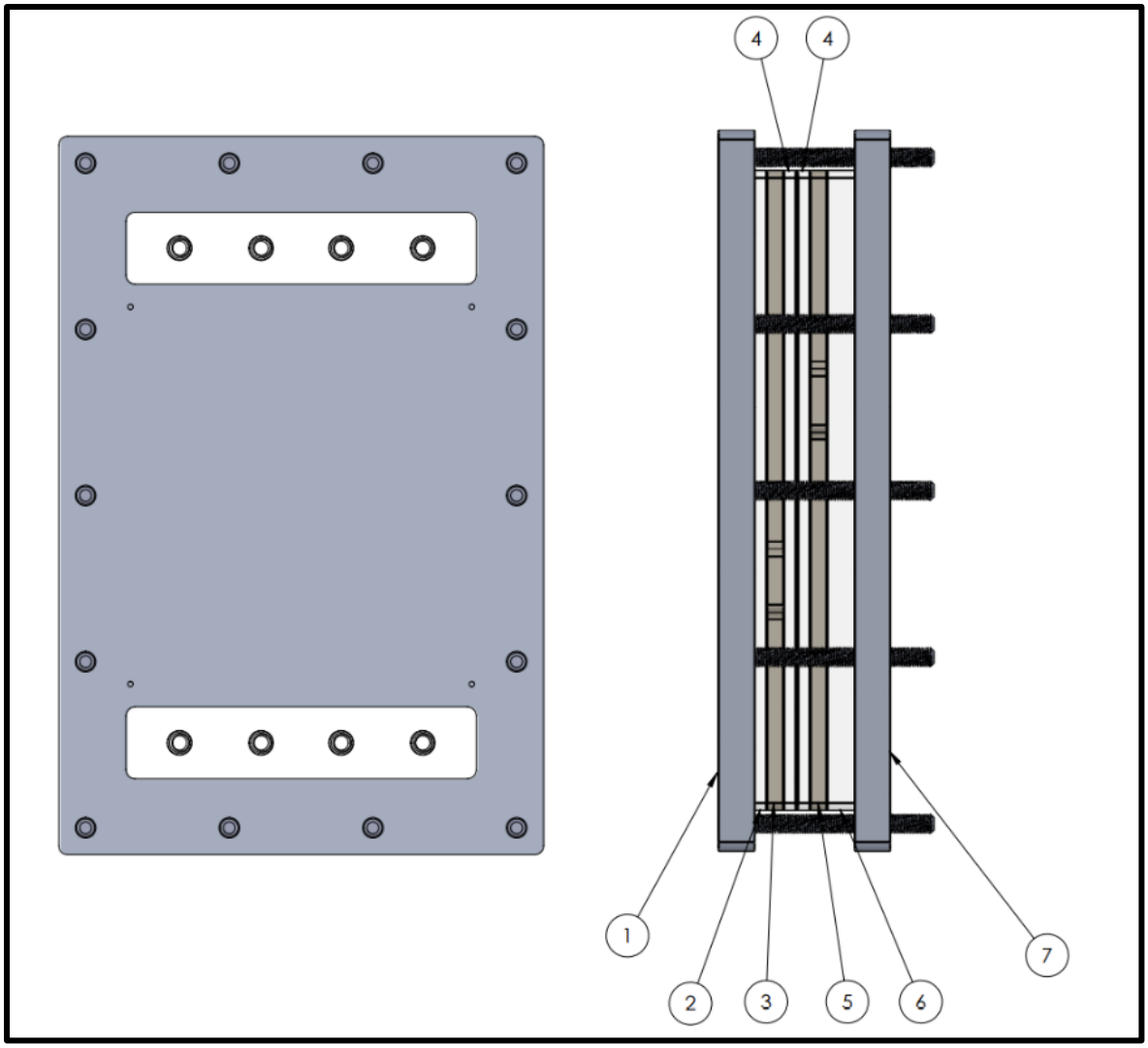

Figure 5.1. Whole-cell assembly with labeled parts description given in Table 5.1. The dimensions of the fully assembled cell are 27 cm x 40 cm x 12 cm. A GDE could fit in between rubber gaskets between parts 3 and 4 or 4 and 5. A membrane would fit between gaskets and the two chosen flow regions (4 and 4 for a two GDE setup, 3 and 4 or 4 and 5 for a single GDE setup, or 3 and 5 for a conventional 3D electrode flow through setup). The openings on the top compression plate are for clearance for NPT connections.

Table 5.1. Description of parts in Figure 1 and their material of construction.

Part Number	Description	Material
1	Base Compression Plate	Aluminum
2	Back Insulator Plate	PVC
3	Cathode Current Collector	Nickel
4	Flow Distributor	PVC
5	Anode Current Collector	Titanium
6	Feed Insulator Plate	PVC
7	Top Compression Plate	Aluminum

All flows are fed through the front of the cell, allowing multiple cells to be stacked in one assembly. Gaskets (not depicted) are employed in between each plate for sealing. This cell can run a GDE at the cathode and anode, resulting in a four-compartment design. This was to allow for the option of using a hydrogen anode with the cathodic reaction to reduce the cell potential significantly. If a conventional 3D anode is desired, one of the flow distributors (4) would be removed from the cell assembly. The flow distributor plate and customizations are displayed in Figure 5.2. Views A and B in Figure 2 show the core flow distributor plate of the cell. These plates are designed to be 6 mm thick so that testing various flow distributions would be easier (i.e., thinner flow inserts could deform more during operation and restrict flow in the cell. View C shows an example of flow distribution inserts (orange), while views D and E show inserts for reducing the cell's active area by half. This can be achieved such that the height of the cell is greater than the width of the cell (view D) or the width of the cell is greater than the height (views E & F). Inserts can be 3D printed using ABS filament allowing for fast and easy customization of these parts including customization of the cell area.

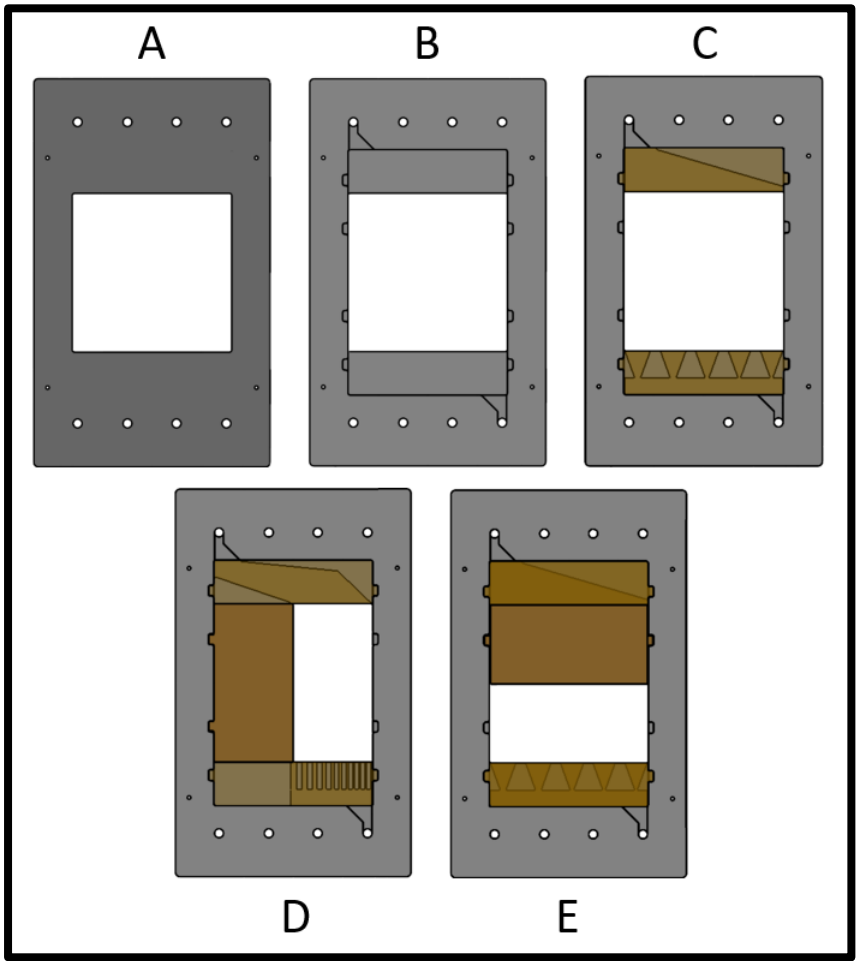

Figure 5.2. Configurations of the flow distributor plate with customizable inserts (orange). The insert shown in E is hollowed to allow flow behind it from the bottom to the top of the cell. A shows the front face of the flow distributor. B shows the back face of a flow distributor where connections with inserts are able to be made. C shows an example of two flow distribution inserts for a 200 cm^2 configuration. D shows two flow distribution inserts and a blinding/compression aid piece for a 100 cm^2 configuration where the electrode is taller than it is wide. E shows two flow distribution inserts and a blinding/compression aid piece for a 100 cm^2 configuration where the electrode is wider than it is tall.

Figure 5.3 displays the current collector plate and how it can be customized. Views A and B in Figure 5.3 show the core current collector plate. These plates are 10 mm thick. The anode is made from titanium, and the cathode is made from nickel. Additionally, the flow holes are lined with fluorinated ethylene propylene (FEP) to avoid shunt current losses. Similar to the flow distributor plate, inserts can be custom-designed for flow distribution on the backside of the current collector (view B). Views C and D show inserts for the current collector to modify the cell's active area by half, although adjusting the dimensions of this plate can change the active area to any value less than 200 cm^2. These inserts retain a recessed groove for a GDE to sit. A further open area of the plate allows for the placement of a conductive material (e.g., stainless steel mesh) to provide additional contact to the GDE on the backside. If a GDE is not desired, any 3D electrode can be placed in this open area on the current collector.

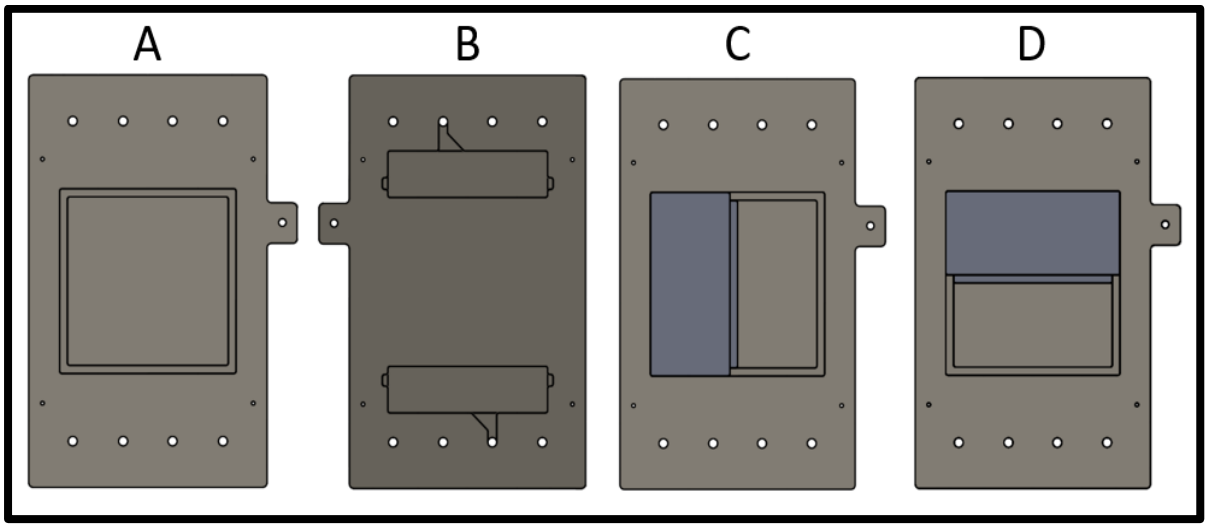

Figure 5.3. Current collector plate with customizable insert for cell area adjustment. The insert shown in D is hollowed to allow flow behind it from the bottom to the top of the cell. A shows the front face of the current collector. B shows the back face of a current collector where connections with inserts are able to be made. C shows a metallic insert that allows for a 100 cm^2 electrode to be used where the electrode is taller than it is wide. D shows a metallic insert that allows for a 100 cm^2 electrode to be used where the electrode is wider than it is tall.

Materials and Chemicals

The same materials used in Chapter 4 were used for the work performed in this chapter. Table C.1 summarizes the suppliers used for the materials and chemicals in this chapter.

Gas Diffusion Layer Explanation and Synthesis

Although Chapter 3 discussed the GDL production method could potentially be reduced to two heating regimes instead of three, we selected two methods from Chapter 3 with characteristics already measured (and vastly different in a few characteristics) to study the GDL with the catalyst layer in Chapter 4. This was done to demonstrate that the GDL can play a large role in the performance of the electrode and should be considered by researchers when performing their studies or comparing multiple studies. This chapter is now using a GDE recipe in Chapter 4 to demonstrate that the results at 10 cm^2 can scale to 200 cm^2. GDL formulation

23 from Chapter 3 was used to synthesize the GDL for the scale-up run in this chapter, which agrees with the formulation for the best performing electrode of the DOE in Chapter 4 (Run 30).

The synthesis method for the GDLs in this study was modified from a patented method.[13] 8.92 mL of PTFE DISP 30 was added to 70 mL of a 1:1 volume IPA:water mixture and stirred for 1 minute before mixing with 15g of Soltex Acetylene black 75%-03 carbon in a Bourgini mixer. After 1 minute of mixing, a dough-like mixture was collected. A rolling pin was used to prepare the dough for a cross rolling technique to obtain the desired thickness where the thickness setting is a discrete numerical factor. A rectangle of about 250 cm^2 was cut from this structure and a paint roller was used to apply PTFE DISP 30 diluted 50% with 1:1 volume IPA:H_2O to the back of the dough. Fibreglast™ 1k plain weave carbon fiber fabric was used as the current collector and placed on top of the PTFE applied layer. A Carver heated press (Model number 4533) was used to press the structure at 140 ^oC and 10.25 Ton for 32.5 minutes. The temperature was then raised to 307.5 ^oC and held at 10.25 Ton for 32.5 minutes. Finally, the temperature was increased to 318 ^oC, and the pressure increased to 13 Ton for 32.5 minutes.

Catalyst Synthesis

The carbon-supported, bimetallic InBi catalyst (50:50 wt %, as in Chapter 4) was prepared in TEG *via* a chemical reduction method. 1.41 g of $InCl_3$ and 1.72 g of $Bi(NO_3)_3 \cdot 5H_2O$ were dissolved in 200 mL of triethylene glycol (TEG) along with 0.98 g of trisodium citrate dihydrate. The mixture was stirred and heated to 60 °C under a N_2 atmosphere until the salts were dissolved. 0.2 g of Vulcan carbon was added to achieve 90 wt% metal supported on carbon, and the mixture was stirred overnight. The resulting suspension was heated to 100 °C, and the N_2 atmosphere was switched to an Ar atmosphere. When the desired temperature was reached, 1.86 g $NaBH_4$ dissolved in 4 mL of water was added over 40 seconds to the reaction mixture. The mixture was left to react at temperature for 15 minutes before being cooled down, filtered, and washed several times with isopropanol and isopropanol/water mixtures.

GDE preparation

A die was used to cut the GDL to the shape required for the cell. The catalyst was sonicated in isopropanol before adding the Nafion™ binder. The amount of Nafion™ added to the ink was calculated based on the mass of catalyst used to make a 20 wt% Nafion™ solution. The ink was then airbrushed onto the GDL, targeting a theoretical metal loading of 0.5 mg_{metal}/cm^2.

Electrolysis

The electrolysis was carried out in the designed 200 cm^2 cell. The anode was a layered Ir/RuO_2 mesh contacted by a Ti backplate, and the cathode was a GDE formulated from our previous studies. A reinforced NafionTM membrane N324 separated the cathode and anode. The anolyte was a 0.5M H_2SO_4 solution, and the catholyte was a 0.5M $KHCO_3$ solution. The anodic reaction was the oxygen evolution reaction (OER). The electrolyte solutions were circulated in the compartments at a flow rate of 1.2 L/min with a peristaltic pump, and CO_2

was fed through the GDE at a flow rate of 1 L/min. The cell was connected to a power supply and operated galvanostatically at a current density of 300 mA/cm^2. Catholyte samples were neutralized with HCl and analyzed for formate with a Perkin Elmer Lambda 35 UV-vis spectrometer.

Results and Discussion

Comsol was used to screen flow distribution designs for their ability to create uniform flow inside the cell. The modeled fluid velocity profile inside the cell with two flow distribution configurations is shown in Appendix D (Figures D.1-D.6). The flow velocity does not appear to be drastically different in the active area region of the cell for the inserts simulated. Therefore, experiments with various flow distribution inserts were not prioritized.

This cell was used to test a 200 cm^2 GDE synthesized from the abovementioned method. The 10 cm^2 GDE recipe that this experiment scaled up showed a current efficiency of 99.4% at a current density of 400 mA/cm^2 for 120 minutes of operation (Run 30 in Chapter 4). However, in a separate, unpublished experiment, when the current density was dropped to 300 mA/cm^2, this electrode achieved 92% current efficiency for 120 minutes. The first run of this scaled-up GDE only lasted for 15 minutes due to high heat generation from the cell, resulting in the electrolyte temperature rising to 55 ^{o}C. This first experiment only used 1.5 L of anolyte and catholyte. A second test was performed with the same electrode using eight liters of anolyte and catholyte contained in an ice bath. It resulted in two hours of additional operation time before the electrolyte temperature reached 55 ^{o}C. Figure 5.4 shows the current efficiency toward formate vs. the combined time of these two 200 cm^2 tests. The corresponding cell potential vs. time is shown in Figure 5.5. Furthermore, a plot of the current efficiency vs applied current, as shown in Chapter 1 (Figure 1.2), with the work contained in Chapters 4 and 5 in this thesis is shown in Figure 5.6.

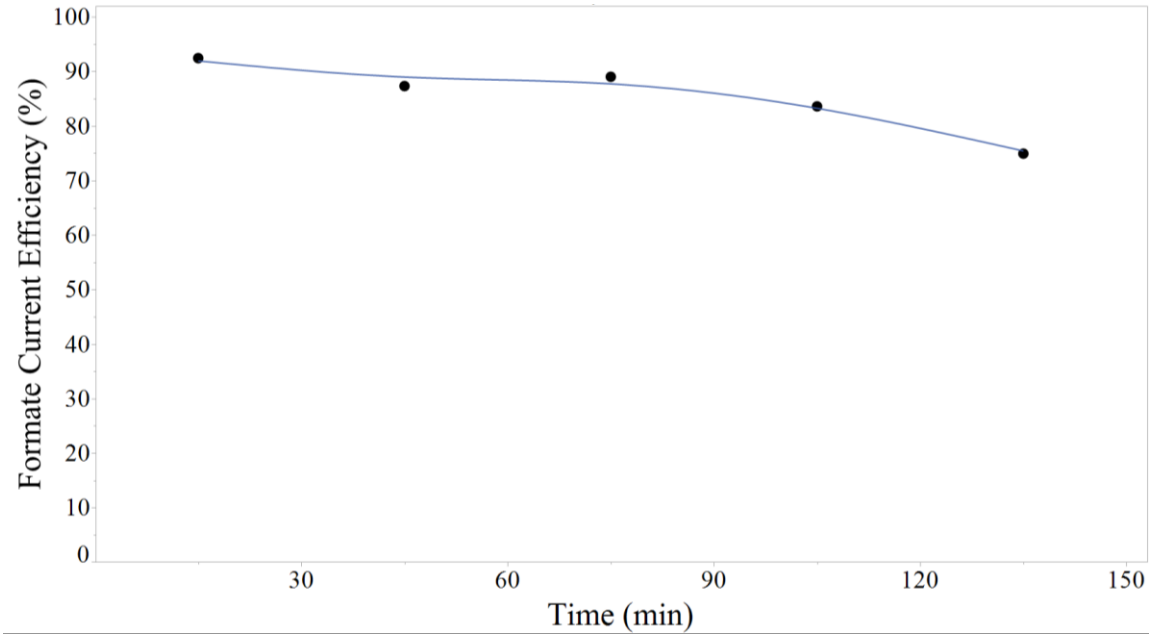

Figure 5.4. The current efficiency of formate vs. time for 200 cm^2 GDE at 300 mA/cm^2. The blue line is drawn to guide the eye.

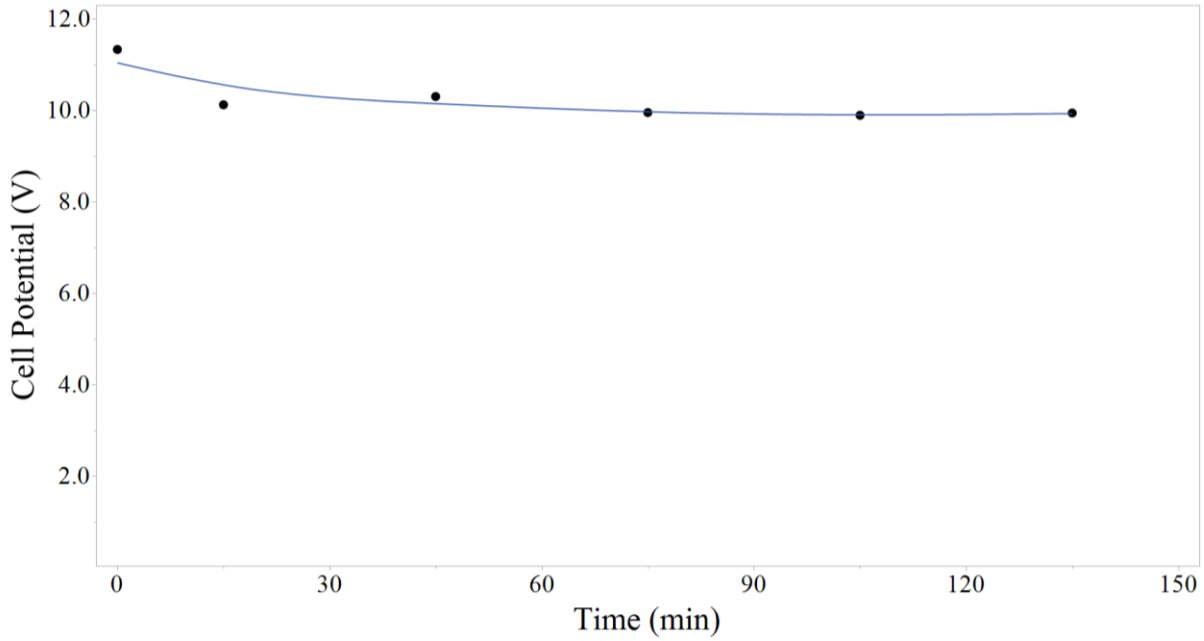

Figure 5.5. Cell potential vs. time for 200 cm^2 GDE at 300 mA/cm^2. The blue line is drawn to guide the eye.

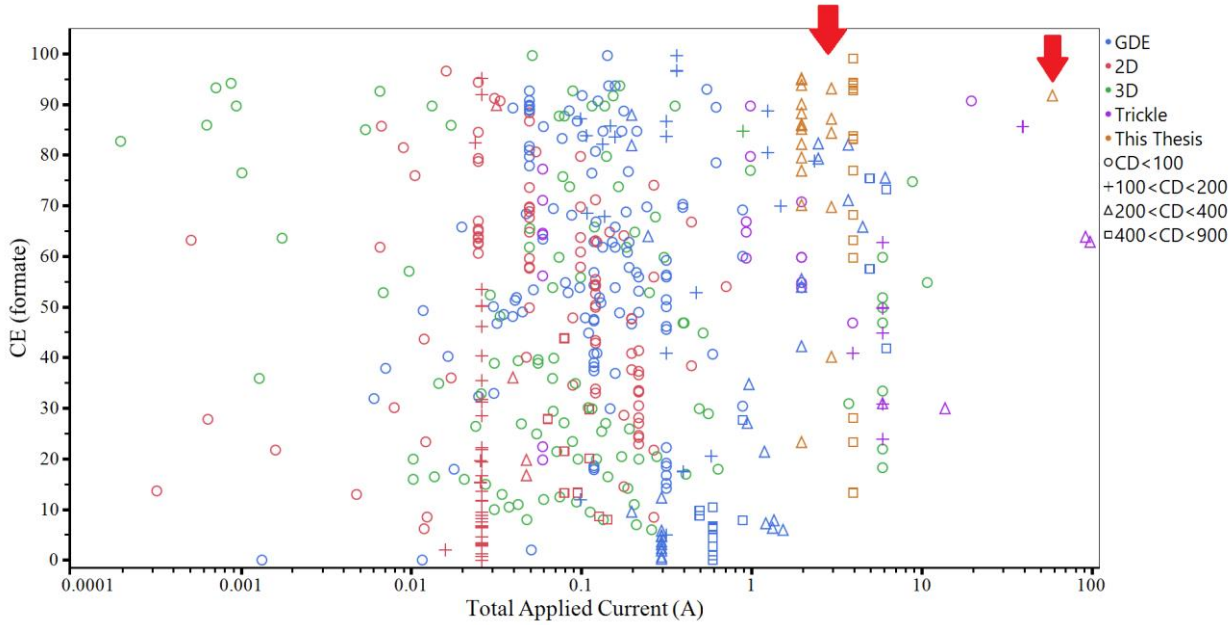

Figure 5.6. Current efficiency vs total applied current for experiments in this thesis overlayed with work reviewed in Chapter 1 (Figure 1.2). Data reported for this thesis at 60A of applied current is shown at the peak performance.

The 200 cm^2 GDE was not operated at 400 mA/cm^2 because the cell potential was nearly double that of the 10 cm^2 electrode. This increase in cell potential is attributed to the large gap of catholyte in the cell of about 9.5 mm, over a 2x increase in gap size from the 10 cm^2 cell (6.35 mm from the flow plate plus 3.15 mm from the gaskets). Consequently, the scaled electrode was only operated at 300 mA/cm^2. It ran at a current efficiency of 92.5% during the first 15-minute experiment. During the second experiment, this electrode achieved 89% current

efficiency for the first 60 minutes before dropping to 75% after a total of 135 minutes of operation.

The first 75 minutes of the scaled electrode operation show very similar current efficiencies to its 10 cm^2 counterpart with less than a 3% difference in current efficiency. However, the larger electrode did not show as good stability as the 10 cm^2 electrode, as seen by the drop in current efficiency at 105 minutes. This is most likely a consequence of the higher cell potential and the higher temperature at which this cell operated. Adapting the flow distributor plate to be about half of the current thickness and using thinner gaskets should help reduce the cell potential. Additionally, including a heat exchanger in the electrolyte tanks to control their temperatures would eliminate the possibility of electrode stability issues due to operating temperature. Nevertheless, this work successfully demonstrates that a GDE can be scaled up without a sacrifice in current efficiency, as seen in other electrolyzer technologies, as shown in Figure 5.6.

Conclusions

GDEs can be a challenge to scale up due to hydrostatic head pressure causing electrode flooding. Most published research on GDEs for CO_2 reduction toward formate is at a scale of 10 cm^2 or less; however, research at larger scales is necessary to understand scaling challenges and eventually achieve a commercial process. There is a lack of commercially available GDE cells for active areas greater than 10 cm^2. Therefore, it was necessary to custom design a cell for GDEs at a larger scale.

Our custom-designed cell featured four compartments, allowing for the possibility of using a hydrogen GDE anode to significantly reduce the cell potential. Additionally, the design allowed for multiple cells to be combined into one stack so that this type of configuration could be tested in the future. The cell's flow distribution and active area were customizable up to 200 cm^2. Although, the custom-designed flow distributions modeled in COMSOL did not appear to significantly change the velocity profile of the electrolyte in the active area of the cell.

The custom cell was used to scale the results from Chapter 4 at 10 cm^2 that showed 99% current efficiency at 400 mA/cm^2. The gap between the GDE and membrane of our 200 cm^2 cell was 9.5 mm, resulting in almost a 2x increase in cell potential from the smaller scale electrode. Consequently, the 200 cm^2 electrode was only operated at 300 mA/cm^2. However, it achieved a current efficiency of 89% for 75 minutes, similar to the performance of the 10 cm^2 electrode at 300 mA/cm^2 (92% current efficiency). Furthermore, the current efficiency of the 200 cm^2 electrode dropped to 75% after 135 minutes of operation, showing lower stability than at the smaller scale. This decrease in stability could be caused by the larger cell potential of the 200 cm^2 cell or the higher operating temperature of the electrolytes (55 ^oC). The InBi catalyst was characterized by Davide Pavesi in Appendix B using differential scanning calorimetry (DSC). Minor peaks associated with bimetallic phases at 66°C, 84 °C, and 107°C were observed on the first cycle (Figure B.5a). These peaks indicate the presence of In_2Bi, InBi, and the eutectic phase.[14] However, during the second cycle (Figure B.5b), these peaks no longer appear. This shows that the InBi catalyst can be transformed when exposed to high

temperatures. Furthermore, the performance of either of the base metals in flow cell benchmarking experiments performed in Appendix B is not as good as the InBi alloy, as shown in Figure B.1. The fact that 1.5 L of electrolyte was heated to 55 ^{o}C in only 15 minutes in these large scale experiments indicates the electrode surface was at a significantly higher temperature than 55 ^{o}C. This elevated temperature could have been enough to cause a transformation of the catalyst, as observed from the DSC characterization work, resulting in a decrease in current efficiency, as seen in the benchmarking experiments in Appendix B.

Further research is required to understand why there was an observed decrease in electrode stability. The gap between the GDE and membrane in the cell can be reduced by using thinner gaskets and reducing the thickness of the flow distributor plate of the cell. Additionally, a better heat exchanger than an ice bath can be used to control the temperature of the electrolytes. Once the electrode stability is addressed, cell stacking should be investigated, as this can also be a challenge in managing pressures between CO_2 and catholyte compartments in the cell.

References

(1) Durst, J.; Rudnev, A.; Dutta, A.; Fu, Y.; Herranz, J.; Kaliginedi, V.; Kuzume, A.; Permyakova, A. A.; Paratcha, Y.; Broekmann, P.; Schmidt, T. J. Electrochemical CO_2 Reduction – A Critical View on Fundamentals, Materials and Applications. *Chim. Int. J. Chem.* **2015**, *69* (12), 769–776, DOI 10.2533/chimia.2015.769.

(2) Oloman, C.; Li, H. Electrochemical Processing of Carbon Dioxide. *ChemSusChem* **2008**, *1* (5), 385–391, DOI 10.1002/cssc.200800015.

(3) Martín, A. J.; Larrazábal, G. O.; Pérez-Ramírez, J. Towards Sustainable Fuels and Chemicals through the Electrochemical Reduction of CO_2 : Lessons from Water Electrolysis. *Green Chem.* **2015**, *17* (12), 5114–5130, DOI 10.1039/C5GC01893E.

(4) Verma, S.; Kim, B.; Jhong, H.-R. "Molly"; Ma, S.; Kenis, P. J. A. A Gross-Margin Model for Defining Technoeconomic Benchmarks in the Electroreduction of CO_2. *ChemSusChem* **2016**, *9* (15), 1972–1979, DOI 10.1002/cssc.201600394.

(5) Huang, Z.; Grim, R. G.; Schaidle, J. A.; Tao, L. The Economic Outlook for Converting CO_2 and Electrons to Molecules. *Energy Environ. Sci.* **2021**, *14* (7), 3664–3678, DOI 10.1039/D0EE03525D.

(6) Philips, M. F.; Gruter, G.-J. M.; Koper, M. T. M.; Schouten, K. J. P. Optimizing the Electrochemical Reduction of CO_2 to Formate: A State-of-the-Art Analysis. *ACS Sustain. Chem. Eng.* **2020**, DOI 10.1021/acssuschemeng.0c05215.

(7) Kaczur, J. J.; Kramer, T. J.; Keyshar, K.; Majsztrik, P.; Twardowski, Z. Process and High Surface Area Electrodes for the Electrochemical Reduction of Carbon Dioxide. US 8,858,777 B2, 2014.

(8) Oloman, C.; Li, H. Continuous Co-Current Electrochemical Reduction of Carbon Dioxide. US 2016/0068974A1, 2016.

(9) Sen, S.; Skinn, B.; Hall, T.; Inman, M.; Taylor, E. J.; Brushett, F. R. Pulsed Electrodeposition of Tin Electrocatalysts onto Gas Diffusion Layers for Carbon Dioxide Reduction to Formate. *MRS Adv.* **2017**, *2* (8), 451–458, DOI 10.1557/adv.2016.652.

(10) Kopljar, D.; Wagner, N.; Klemm, E. Transferring Electrochemical CO_2 Reduction from Semi-Batch into Continuous Operation Mode Using Gas Diffusion Electrodes. *Chem. Eng. Technol.* **2016**, *39* (11), 2042–2050, DOI 10.1002/ceat.201600198.

(11) Higgins, D.; Hahn, C.; Xiang, C.; Jaramillo, T. F.; Weber, A. Z. Gas-Diffusion Electrodes for Carbon Dioxide Reduction: A New Paradigm. *ACS Energy Lett.* **2019**, *4* (1), 317–324, DOI 10.1021/acsenergylett.8b02035.

(12) Burdyny, T.; Smith, W. A. CO_2 Reduction on Gas-Diffusion Electrodes and Why Catalytic Performance Must Be Assessed at Commercially-Relevant Conditions. *Energy Environ. Sci.* **2019**, *12* (5), 1442–1453, DOI 10.1039/C8EE03134G.

(13) Philips, M. F.; Ansovini, D.; Figueiredo, M. C. C.; Krasovic, J. Method for the Preparation of a Gas Diffusion Layer and a Gas Diffusion Layer Obtained or Obtainable by Such Method. WO2020165074A1, 2020.

(14) Okamoto, H.; Schlesinger, M. E.; Mueller, E. M. Bi (Bismuth) Binary Alloy Phase Diagrams. *Alloy Phase Diagrams*. ASM International April 2016, p 0, DOI 10.31399/asm.hb.v03.a0006150.